RSC Advances

PAPER

View Article Online
View Journal | View Issue

Check for updates

Cite this: *RSC Adv.*, 2021, **11**, 2616

Enhanced ferroelectric and piezoelectric performance of $(Ba_{0.85}Ca_{0.15})(Zr_{0.1}Ti_{0.9})O_3$ lead-free ceramics upon Ce and Sb co-doping

Weijie Zheng,[a] Jiaqi Lin,[ab] Xinmei Liu, *[a] Wenlong Yang *[a] and Yuanshuo Li[a]

Received 6th November 2020
Accepted 15th December 2020

DOI: 10.1039/d0ra09441b

rsc.li/rsc-advances

$(Ba_{0.85}Ca_{0.15})(Zr_{0.1}Ti_{0.9-x}Ce_x)O_3+ySb$ (abbreviated as $BCZTC_xS_y$) ceramics were prepared by the conventional solid-state reaction. The effect of the co-doping of Ce and Sb on the phase structure, microstructure, dielectric, and ferroelectric and piezoelectric performances of $BCZTC_xS_y$ ceramics were investigated systematically. The results indicated that the obtained ceramics are composed of coexisting rhombohedral and tetragonal phases. Significant improvements were also observed in the growth of grain, relative density, as well as electrical performance. After co-doping 0.05 mol% Ce and 0.10 mol% Sb, the sizes of crystalline grains reached the maximum. The following optimal properties were obtained: $\varepsilon_r = 2353$, $\tan\delta = 0.026$, $T_c = 109.4$ °C, $P_{max} = 17.65$ μC cm^{-2}, $P_r = 10.43$ μC cm^{-2}, $E_c = 2.88$ kV cm^{-1}, $S_{max} = 0.125\%$, $d^*_{33} = 417$ pm V^{-1}, $d_{33} = 372$ pC N^{-1}. With the increase in dopants, the diffuseness γ increased from 1.663 to 1.733, indicating a more relaxed ferroelectric characteristic. All improvements show that BCZT ceramics co-doped with Ce and Sb could be promising candidates in lead-free devices.

Introduction

Piezoelectric materials are considered as one of the essential functional materials and have been widely applied in transducers, sensors and acoustic wave devices.[1–3] However, currently commercial piezoelectric materials contain a large amount of lead element, such as $Pb(Zr_{0.3}Ti_{0.7})O_3$ (PZT) and $0.67Pb(Mg_{1/3}Nb_{2/3})O_3$–$0.33PbTiO_3$ (PMNT), which intrinsically limited by their toxicity.[4,5] Therefore, lead-free piezoelectric materials are urgently required for the advocation of environmentally-friendly concepts.

In the past decade, tremendous efforts have been devoted to fabricating lead-free ceramic systems, such as $K_{0.5}Na_{0.5}NbO_3$ (KNN), $Bi_{0.5}Na_{0.5}TiO_3$ (BNT), $BaTiO_3$ (BT) and $BiFeO_3$ (BFO).[6–10] Among them, BT-based ceramics have received widespread attention due to their stable chemical properties, low preparation cost, large dielectric permittivity (ε_r) and low leakage current.[11,12] However, in actuality, the BT-based ceramics are not the ideal piezoelectric materials, and the low piezoelectric coefficient ($d_{33} = \sim$190 pC N^{-1}) compromises the commercialization of their applications.[13,14] In order to enhance the piezoelectric properties, numerous strategies have been adopted such as sintering with new technology, modifying ceramics with dopants, or providing new ways to facilitate the poling process.[13–19] The ultrahigh piezoelectric effect is generally derived from the morphotropic phase boundary (MPB) in the BT-based system.[20] As $BaTiO_3$ has rich phase transition and unit cell structure types, the modification of BT to form MPB to improve piezoelectric performance is a promising strategy.[21] Ren *et al.* have found an MPB region by utilizing Ca^{2+} and Zr^{4+} ions to modify the $BaTiO_3$ ceramic. $(Ba_{0.85}Ca_{0.15})(Zr_{0.1}Ti_{0.9})$(BCZT) shows fascinating piezoelectric performance ($d_{33} \sim 600$ pC N^{-1}), which is comparable to that of the commercial PZT ceramics. According to the results from the Landau–Devonshire phenomenological theory and *ab initio* calculations, the origin of the piezoelectric enhancement is the flattening of a free-energy profile.[22–24]

Although BCZT has not been widely applied in industry, high piezoelectric response and low cytotoxicity make it a promising system for electronic devices, biomedical applications and energy harvesters for the wearable.[25,26] In order to improve the comprehensive electrical performance of BCZT ceramics, extensive efforts have been devoted to the modification of BCZT ceramics. For example, Wang *et al.* investigated the effects of numerous rare-earth elements (including Dy, Er, Eu, Ho, Pr and Sm) on the electrical properties of ceramics, and enhanced piezoelectric properties are varied from 475 to 521 pC N^{-1}.[27] Compared with other rare-earth elements, Ce is an attractive one that exhibits a variety of valences, which can be widely used to improve the electrical properties of ceramics. Bijalwan *et al.* obtained a large piezoelectric response ($d_{33} = 501$ pC N^{-1}) and a higher Curie temperature ($T_c = 108.1$ °C) when 0.13 mol% Ce was doped into BCZT ceramics.[28] Raziye *et al.* obtained the highest converse piezoelectric coefficient ($d^*_{33} = 1189$ pm V^{-1}) in BCZT–0.05 mol% Ce.[29] For ABO_3-type perovskite piezoelectric materials, the spontaneous polarization mainly originates from the displacement of the B-site cations within the $[BO_6]$

[a]*Department of Applied Science, Harbin University of Science and Technology, Harbin 150080, P. R. China. E-mail: liuxinmei.1990@163.com; yangwenlong1983@163.com; Tel: +86-451-8639-2428*

[b]*Key Laboratory of Engineering Dielectrics and Its Application, Ministry of Education, Harbin University of Science and Technology, Harbin 150080, P. R. China*

Open Access Article. Published on 12 January 2021. Downloaded on 12/9/2025 6:57:55 AM.
This article is licensed under a Creative Commons Attribution-NonCommercial 3.0 Unported Licence.

© 2021 The Author(s). Published by the Royal Society of Chemistry

Open Access Article. Published on 12 January 2021. Downloaded on 12/9/2025 6:57:55 AM.
This article is licensed under a Creative Commons Attribution-NonCommercial 3.0 Unported Licence.

octahedra.[30] Therefore, it is a potential strategy to enhance the electrical performance of BCZT ceramics by utilizing Ce^{4+} ions to replace B-site Ti^{4+} ions. Nevertheless, some Ce^{4+} will turn to Ce^{3+} during the sintering process, then occupy the A-site, and B-site vacancies appear in the ceramic due to the stoichiometric ratio.

In order to avoid the degradation of electrical performance, compensation for the B-site vacancies is urgently required. In the modification of KNN-based ceramics, Sb with high Pauling electronegativity leads to significant improvements in the piezoelectric performance.[31,32] When donor ions were added to ceramics, the oxygen vacancy concentration was restricted. As a result, the pinning of domains is reduced and the domain wall motion is promoted, which improves the electrical properties of ceramics.

In this study, we utilized the Ce synergizing with Sb to enhance the electrical properties of BCZT ceramics.

First, $(Ba_{0.85}Ca_{0.15})(Zr_{0.1}Ti_{0.9-x}Ce_x)O_3$+$y$Sb (abbreviated as $BCZTC_xS_y$, $0 \le x \le 0.15$ mol% and $0 \le y \le 0.10$ mol%) ceramics were prepared by the conventional solid solution processing route. The effects of Ce and Sb on the microstructure, dielectric, ferroelectric and piezoelectric of ceramics were studied, systematically. The diffusion behavior of the samples was analyzed through the correctional Curie–Weiss law. Benefiting from the grain coarsening and the restriction of the oxygen vacancy, the $BCZTC_xS_y$ ceramics exhibited improved ferroelectric and piezoelectric performance. This study can provide an experimental basis for further modification of BCZT ceramics. The enhanced piezoelectric performance makes BCZT a potential candidate for the fabrication of lead-free devices.

Experimental procedures

Raw materials

Analytical-grade carbonate and metal oxide powders of $BaCO_3$ (99.00%), $CaCO_3$ (99.00%), TiO_2 (98.00%) and ZrO_2 (99.00%) were purchased from Sinopharm Chemical Reagent Co., Ltd. Sb_2O_5 (99.00%) was purchased from Shanghai Macklin Biochemical Co., Ltd. CeO_2(99.00%) was purchased from Tianjin Guangfu Fine Chemical Research Institute.

Preparation of BCZT

$(Ba_{0.85}Ca_{0.15})(Zr_{0.1}Ti_{0.9-x}Ce_x)O_3$+$y$Sb (abbreviated as $BCZTC_xS_y$, $0 \le x \le 0.15$ mol% and $0 \le y \le 0.1$ mol%) ceramics were prepared by the conventional solid solution processing route. First, $BaCO_3$, $CaCO_3$, TiO_2, ZrO_2, Sb_2O_5 and CeO_2 were mixed according to the stoichiometric ratio through planetary ball-milling in ethanol for 24 h. Then, the corresponding mixtures were calcined at 1200 °C for 4 h in an oxygen atmosphere, followed by another ball-milling for 24 h, and then dried at 60 °C for 12 h. The dried mixtures were granulated with appropriate polyvinyl alcohol (PVA) as the binder and pressed into disks of 13 mm in diameter and 1 mm thickness. Finally, the pellets were sintered at 1430 °C for 4 h in air. After cooling naturally, the as-sintered pellets were polished using a silicon carbide paper, both the surfaces of ceramics were coated with silver as electrodes.

Characterization and electrical property tests

X-ray diffraction (XRD) data were collected by using an X-ray diffractometer (DX-2700B, Haoyuan Instrument, China) with Cu K_α radiation of wavelength $\lambda = 0.1540$ nm. The optical micrograph (OLYMPUS BX51) was employed to identify the microstructure of materials. X-ray photoelectron spectroscopy (XPS) data were recorded using an Escalab 250Xi X-ray photoelectron spectrometer (Thermo Fisher Scientific). The volume density of the sample was measured by the Archimedes' method. The room-temperature dielectric properties were measured with a precision impedance tester (Agilent E4294A, Agilent Technologies, CA, USA). The dielectric temperature spectra of the sample were recorded using an LCR meter (Agilent E4980A, Agilent Technologies, CA, USA) under an increasing temperature range from 40 to 180 °C. The ferroelectric hysteresis loops (P–E) and electric field-induced strain loops (S–E) were measured using a ferroelectric tester (Radiant Multiferroic, USA). Then, the converse piezoelectric coefficient (d^*_{33}) was calculated based on the S–E spectrum. The piezoelectric constant d_{33} was obtained with a quasi-static d_{33} meter (ZJ-4AN, Institute of Acoustics, Beijing, China) after the samples were poled under a DC field of 3.5 kV mm^{-1} for 30 min at 60 °C.

Results and discussion

In attempts to detect the crystal structure of the obtained samples, $(Ba_{0.85}Ca_{0.15})(Zr_{0.1}Ti_{0.9-x}Ce_x)O_3$ +ySb ceramics (abbreviated as $BCZTC_xS_y$, $0 \le x \le 0.15$ mol% and $0 \le y \le 0.1$ mol%) were characterized *via* XRD. As shown in Fig. 1(a), only the perovskite phase is observed and no impurity phases can be detected for all the samples, indicating that Ce and Sb diffused into the lattice to form a solid solution. Furthermore, crystallographic indexing and the splitting peak near 45° can be observed in Fig. 1(b), which implies the coexisting structures of orthorhombic with rhombohedral phases in the ceramic samples. Due to the similar ionic radii of Sb^{5+} (0.600 Å) and Ti^{4+} (0.605 Å), the in-plane lattice parameters (3.999 Å and 3.998 Å) of the ceramic sample show no significant changes after Sb doping. Considering that Ce exhibit +3 and +4 valences, the occupation mechanism for samples that are doped with Ce is complicated, Although CeO_2 is used as a dopant, Ce^{3+} ions might be generated during the sintering process.[33] Upon the introduction of 0.10 mol% Ce into the BCZT ceramic, the in-plane lattice parameter increased from 3.999 Å to 4.002 Å, implying that most of the Ce occupies B-site in the samples. The ionic radius of Ce^{4+} (0.870 Å) is bigger than that of Ti^{4+} (0.605 Å), whereas the ionic radius of Ce^{3+} (1.340 Å) is smaller than that of Ba^{2+} (1.610 Å). The B-site occupation is considered as the dominant form for Ce^{4+} in the Ce-doped BCZT ceramics.

The surface micrographs of ceramic samples are shown in Fig. 2. All the samples demonstrate an irregularly elliptical grain. With the increase in the number of dopants, the bonding between the grains becomes tighter, indicating the reduction in the number of pores in the sample. In order to study the effect of dopants on the microstructure of the ceramics, the statistic distribution of the grain size for more than 900 grains in every

Open Access Article. Published on 12 January 2021. Downloaded on 12/9/2025 6:57:55 AM.
This article is licensed under a Creative Commons Attribution-NonCommercial 3.0 Unported Licence.

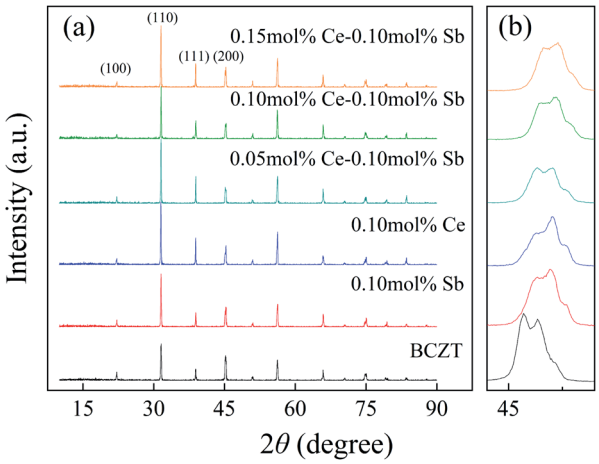

Fig. 1 (a) XRD patterns of BCZT ceramics prepared by co-doping with Ce and Sb and (b) enlarge patterns near 45°. All the measurements were conducted at room temperature.

sample was investigated. The grain size distribution maps are shown in Fig. 3. It was found that dopants can significantly enlarge the grain size of the samples. It can be seen in Fig. 3(a)–(e) that when 0.05 mol% Ce and 0.10 mol% Sb were co-doped into the BCZT sample the average grain size grew from 11.10 μm to 13.51 μm with a standard deviation of 5.93.

During sintering, titanium was easily enriched at grain boundaries, and the impurity phases (such as $BaTi_2O_5$, $BaTi_3O_7$) were formed.[34] The impurity phases converted back to $BaTiO_3$ during the cooling process, and then generated numerous oxygen vacancies and barium vacancies. Compared to the inside grains, the oxygen vacancies would rather accumulate at grain

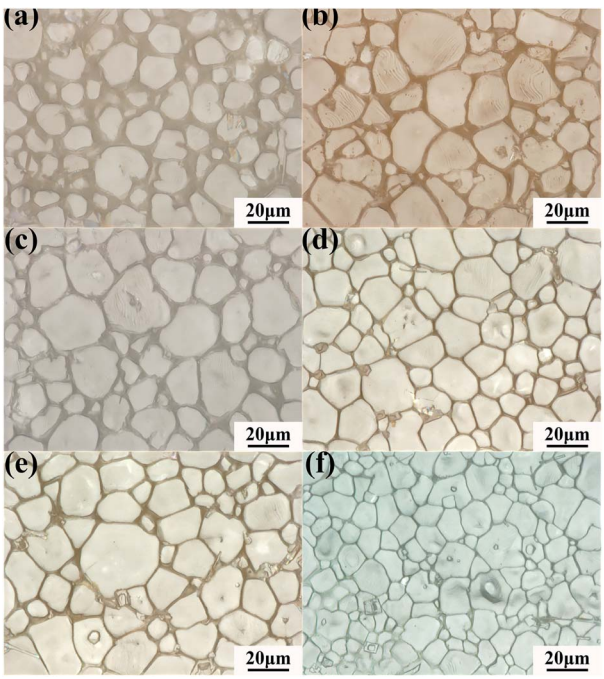

Fig. 2 Surface morphologies of $BCZTC_xS_y$ ceramics: (a) BCZT; (b) $x = 0.10$; (c) $y = 0.10$; (d) $x = 0.05$, $y = 0.10$; (e) $x = 0.10$, $y = 0.10$; (f) $x = 0.15$, $y = 0.10$.

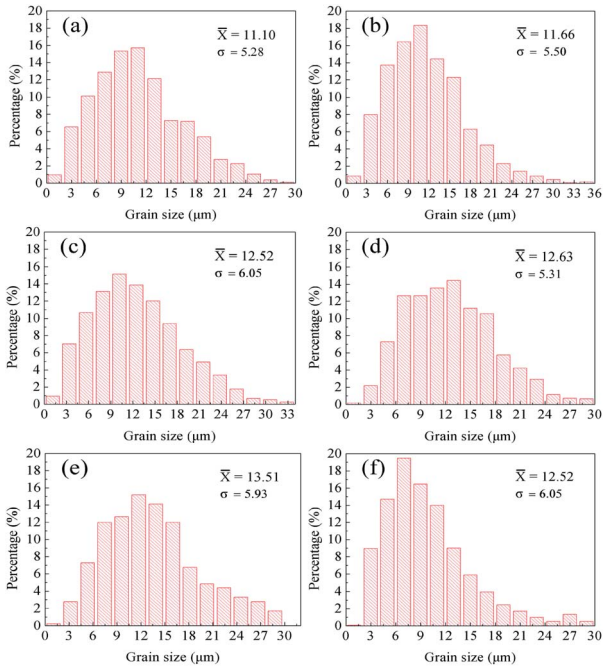

Fig. 3 Grain size distribution in $BCZTC_xS_y$ ceramics: (a) BCZT; (b) $x = 0.10$; (c) $y = 0.10$; (d) $x = 0.05$, $y = 0.10$; (e) $x = 0.10$, $y = 0.10$; (f) $x = 0.15$, $y = 0.10$.

boundaries. The good thermal stability of oxygen vacancies at grain boundaries was considered to hinder the growth of grains.[35] When Ce and Sb were used as dopants for the donor doping of ceramics, the barium vacancies were generated inside the grain. The barium vacancies inside the grains facilitate the diffusion of ions. Moreover, the oxygen vacancy concentration on grain boundaries would be restricted. This can be attributed to the increase in barium ions at grain boundaries, preventing the generation of the impurity phase. Nevertheless, excessive Ce doping would restrain the growth of grain. Because CeO_2 will precipitate at the grain boundaries, thus causing grain refinement.

To determine if the oxygen vacancy concentration in BCZT was restricted by Ce doping, XPS for the pure BCZT and 0.10 mol% Ce-doped BCZT were measured. The XPS spectra of O 1s binding states are shown in Fig. 4. The curve can be fitted with two peaks of the binding energy centered at 529.3 eV and 531.1 eV. The peak at 529.1 eV corresponds to the lattice oxygen and the peak at 531.1 eV is assigned to oxygen vacancies.[36] When 0.10 mol% Ce was doped into BCZT, the relative density ratio of vacancy oxygen ($O_{Vacancy}/O_{Lattice}$) was decreased from 1.54 to 1.04. This result undoubtedly indicates that Ce doping in BCZT would restrict the oxygen vacancy concentration.

Density is closely related to the grain size and pores for ceramics. Fig. 5 shows the relative density and volume density for ceramic samples with the co-doping of Ce and Sb. When 0.05 mol% Ce and 0.10 mol% Sb were co-doped into the ceramic, the optimal relative density could reach 93.52%. The increasing relative density may have been caused by the grain growth, which reduced the pores and increased the unit cell volume of Ce and Sb co-doped ceramic samples.

© 2021 The Author(s). Published by the Royal Society of Chemistry

Open Access Article. Published on 12 January 2021. Downloaded on 12/9/2025 6:57:55 AM.
This article is licensed under a Creative Commons Attribution-NonCommercial 3.0 Unported Licence.

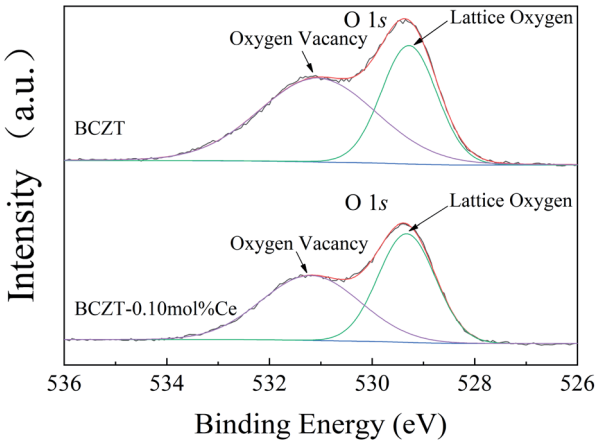

Fig. 4 XPS spectra of O 1s binding states for BCZT and BCZT–0.10 mol% Ce.

In order to investigate the influence of dopants on the dielectric performance, the frequency-dependent dielectric permittivity (ε_r) for BCZTC$_x$S$_y$ ceramics was measured at room temperature. As depicted in Fig. 6, all samples exhibiting high ε_r. Also, ε_r decreased with the increase in frequency. For BCZT ceramics, the ε_r value is mainly contributed by the bulk and domain wall motion: $\varepsilon_r = \varepsilon_{r\text{-vol}} + \varepsilon_{r.wall}$.[37]

According to the dielectric polarization theory, the micro-polarization mechanism of bulk ceramics involves three types: electron displacement polarization, ion displacement polarization and turning-direction polarization. Due to the different polarization mechanisms, ε_r was varied at different frequencies. At lower frequencies, all three polarization mechanisms contribute to ε_r, resulting in a large ε_r value. As the frequency went up to 10^6 Hz, the turning of the electric dipole moment could not keep up with the increase in the electric field frequency. Thus, ε_r was decreased.

Moreover, the motion of the domain wall under an alternating electric field cannot be ignored. To reduce the system energy in polycrystals, multiple electrical domains would be formed inside the grain. The domain wall vibrates at its equilibrium position under an alternating electric field, which increases capacitance. As the electric field frequency was gradually increased, the domain wall would fail to move synchronously. As a result, the ε_r value was decreased.

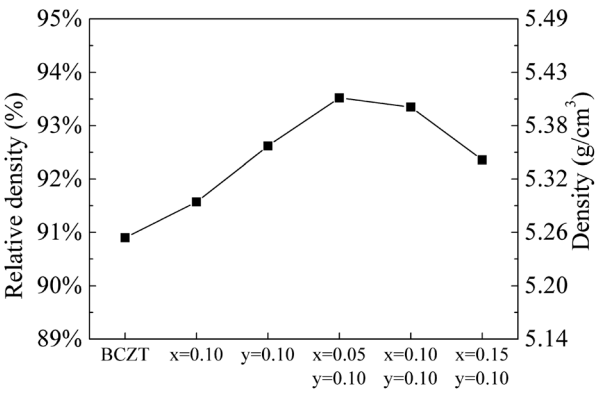

Fig. 5 Relative density and density of BCZTC$_x$S$_y$ ceramics.

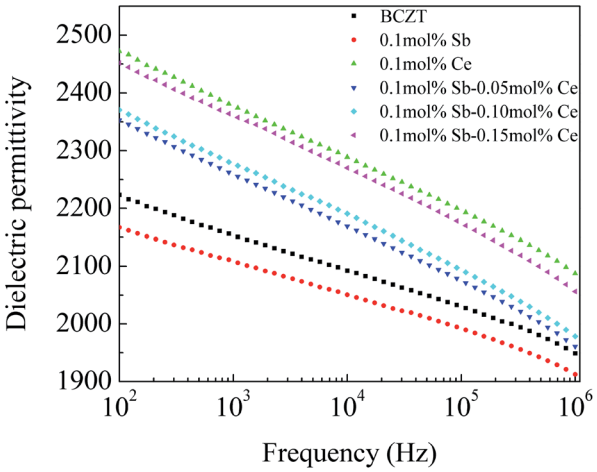

Fig. 6 Frequency-dependent dielectric permittivity of BCZTC$_x$S$_y$ ceramics at room temperature.

Compared to the undoped ceramic, ε_r for sample with the 0.10 mol% Sb-doped sample slightly decreased. It may have been caused by the reduction of interfacial polarization and domain wall motions. As shown in Fig. 2(b) and 3(b), the introduction of 0.10 mol% Sb facilitates the grain growth. The tight bonding between grains then reduced the interface concentration and restricted domain wall motion. When Ce was doped into the samples, the lattice distortion and generated cation vacancies increased the spontaneous polarization and facilitated domain inversion. As a result, ε_r was increased.

The frequency-dependent dielectric losses (tan δ) for BCZTC$_x$S$_y$ ceramics at room temperature are measured. As shown in Fig. 7, the dielectric loss of all ceramic samples first decreased slightly with the increase in frequency then increased rapidly. The main reason for the dielectric loss at a low frequency is the resistance caused by the electric dipole turning and the friction of the domain wall motion.[38] The turning-

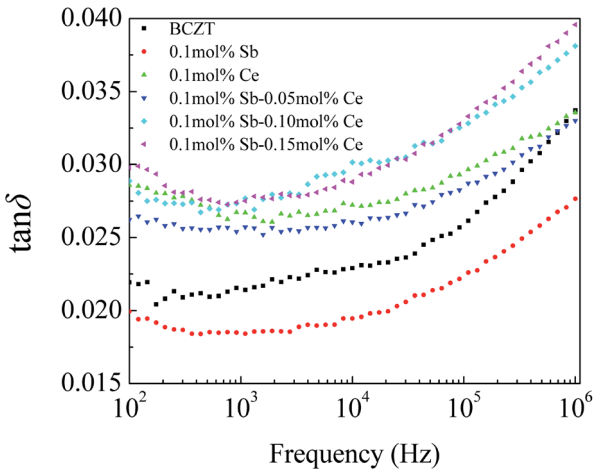

Fig. 7 Frequency-dependent dielectric loss of BCZTC$_x$S$_y$ ceramics at room temperature.

Open Access Article. Published on 12 January 2021. Downloaded on 12/9/2025 6:57:55 AM.
This article is licensed under a Creative Commons Attribution-NonCommercial 3.0 Unported Licence.

direction polarizations become weaker as the frequency gradually increases. As a result, the dielectric loss is slightly reduced. However, at higher frequencies, the domain wall frictional movement would increase the dielectric loss.

Compared to that for undoped ceramic sample, the dielectric loss for 0.10 mol% Sb-doped sample is lower. This contrast could be explained by increased grain size, increased domain size and restriction of the friction between the domain walls. Moreover, the decreased intergranular porosity leads to a decrease in the conductivity loss. When Ce co-doped into the samples, dielectric loss was increased. This behavior can be attributed to the lattice distortion, which promotes the domain wall motion.

To investigate the phase structure variation of ceramic samples with temperature, we measured temperature-dependent dielectric permittivity at the frequency of 1 kHz for $BCZTC_xS_y$. As shown in Fig. 8, the Curie temperature (T_c) of the sample rises to 110.2 °C and 109.1 °C when 0.10 mol% Ce and Sb were doped, respectively, into the BCZT ceramic.

The increase in T_c indicates the improved stability of the ceramic when used at room temperature. According to Fig. 2 and 3, dopants can effectively facilitate the growth of grains, which benefits the release of internal stress for grains, thus increasing T_c.[39] Nevertheless, dopants will increase the concentration of cation vacancies, which reduces the stability of oxygen octahedron.[21] As a result, T_c decreased slightly with the increase in Ce doping. Compared with T_c for the undoped BCZT ceramics, T_c for the Ce and Sb co-doped ceramic was elevated. Moreover, the peak for dielectric T_c was broadened. In order to quantitatively characterize the degree of the diffuse behavior, the modified Curie–Weiss law was employed in this study,[40]

$$\frac{1}{\varepsilon} - \frac{1}{\varepsilon_m} = \frac{(T - T_m)^\gamma}{C} \quad (1)$$

where ε_m is the maximum permittivity, C is the modified Curie–Weiss constant, and γ value ranges from 1 (normal ferroelectric) to 2 (typical relaxer ferroelectric). According to temperature-dependent dielectric permittivity at 10 kHz, the parameter γ can be obtained by the slope of $\ln(1/\varepsilon - 1/\varepsilon_m)$ *versus* $\ln(T - T_m)$,

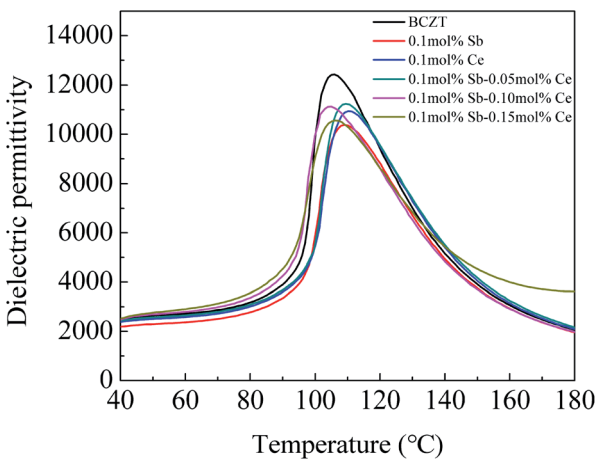

Fig. 8 Temperature dependence of dielectric permittivity for $BCZTC_xS_y$ ceramics at 1 kHz.

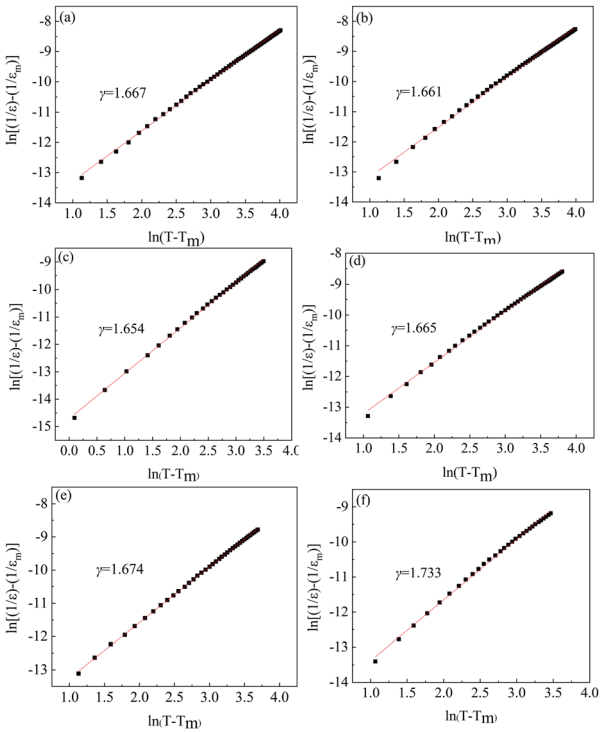

Fig. 9 Linear fitted $\ln[(1/\varepsilon) - (1/\varepsilon_m)]$ as a function of $\ln(T - T_m)$ for $BCZTC_xS_y$ ceramics at 10 kHz: (a) BCZT; (b) $x = 0.10$; (c) $y = 0.10$; (d) $x = 0.05$, $y = 0.10$; (e) $x = 0.10$, $y = 0.10$; (f) $x = 0.15$, $y = 0.10$.

as shown in Fig. 9. It can be observed that γ of the pure BCZT sample is 1.667 and increases to 1.733 with 0.10 mol% Sb and 0.15 mol% Ce co-doping. The increase in the value of γ indicates that the ceramics exhibit more relaxed ferroelectric characteristics. The doping of Ce and Sb leads to a cation disorder in the perovskite unit cell, which elevates the stability of polar nanoregions (PNRs). In addition, macrodomains could be divided into microdomains due to the increase in the PNR concentration. Thus, the ceramics show a more relaxer-like behavior.[41]

The hysteresis loops, ferroelectric parameter remnant polarization (P_r) and coercive field (E_c) of $BCZTC_xS_y$ ceramics measured at room temperature are shown in Fig. 10(a) and (b), respectively. It can be observed that all the *P*–*E* loops are saturated, and P_r can be obviously improved by dopants. When 0.10 mol% Sb and 0.05 mol% Ce were co-doped into ceramic, P_r was increased from 6.67 to 10.09 μC cm^{-2} and E_c was decreased to a minimum 2.87 kV cm^{-1}. All the results indicate the enhanced ferroelectricity of BCZT.

The enhanced P_r of Ce and Sb co-doped ceramics may have been caused by the increase in the grain size. For ferroelectrics, the proportion of grains contributing to polarization reverses can be expressed as[42]

$$f = f_0[1 - e^{-G_a d^\beta / kT}] \quad (2)$$

where d is the grain size, and G_a is a constant used to describe the grain anisotropy energy density. Therefore, f is only relevant to the grain size d. According to Fig. 2 and 3, dopants can promote the grain growth and then enhance the ferroelectricity.

© 2021 The Author(s). Published by the Royal Society of Chemistry

Open Access Article. Published on 12 January 2021. Downloaded on 12/9/2025 6:57:55 AM.
This article is licensed under a Creative Commons Attribution-NonCommercial 3.0 Unported Licence.

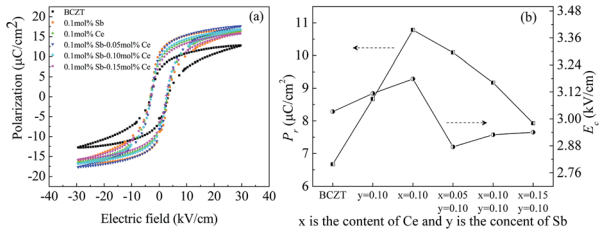

Fig. 10 Room temperature ferroelectricity of $BCZTC_xS_y$ ceramics: (a) electric hysteresis loops (b) P_r and E_c as a function of Ce and Sb contents.

Moreover, the coarsening of grain elevates the domain width, and reduces the grain boundaries, which is beneficial to the continuous inversion of polarization. However, with the increase in the concentration of dopants, the PNRs generated inside the grain were increased. The appearance of PNRs makes the domain structure more complicated, resulting in the reduction of P_r and E_c for samples.

In order to explore the effect of dopants on the piezoelectric performance, the unipolar S–E loops at 30 kV cm^{-1} and the converse piezoelectric coefficient (d^*_{33}) were studied, and the data are shown in Fig. 11(a) and (b), respectively. It is can be seen that the unipolar positive strain is enhanced when ceramic is co-doped with Ce and Sb. The ceramic co-doping with 0.05 mol% Ce and 0.10 mol% Sb shows the maximum value of 0.125%, indicating a significant improvement in the piezoelectric properties of BCZT ceramics. In addition, d^*_{33} can be calculated by the unipolar S–E loops, which are shown in Fig. 11(b). All the result indicates that the dopants improve the d^*_{33} of ceramics, and the 0.05 mol% Ce and 0.10 mol% Sb co-doped ceramic show the optimum value of 417 pm V^{-1}.

The room temperature piezoelectric coefficient (d_{33}) of $BCZTC_xS_y$ ceramics poled under a DC field of 3.5 kV cm^{-1} is shown in Fig. 12. It can be found that dopants show obvious enhancement for the d_{33} of ceramics. The ceramics with 0.05 mol% Ce and 0.10 mol% Sb co-doped exhibit an optimal piezoelectric coefficient d_{33} of 372 pC N^{-1}. The improved piezoelectric performance may have resulted from two reasons. The first reason is that more 90° domains were formed in the grains due to the internal stress of ceramics released with the increase in the grain size.[43] Moreover, grain coarsening increases the domain width and size. The other reason is the restriction of the oxygen vacancy concentration, which can reduce the pinning of domains and promote the domain wall

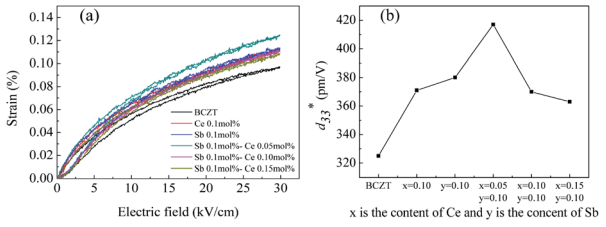

Fig. 11 (a) Unipolar S–E loops and (b) d^*_{33} of Ce and Sb co-doped ceramics.

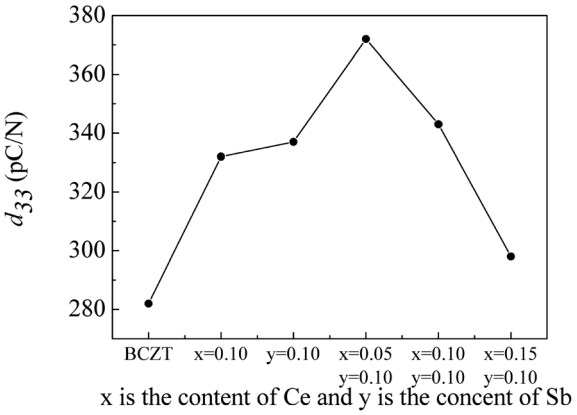

Fig. 12 Piezoelectric coefficient of Ce and Sb co-doped ceramics.

motion. In addition, the appearance of PNRs can reduce E_c, which then makes the samples easier for polarization under the electric field. However, when an excessive dopant was applied, the grain size would be reduced and more PNRs would be formed in grains. As a result, the growth of domains was restricted, which reduced the piezoelectric performance of ceramics.

Conclusions

In this study, we utilized Ce to synergize with Sb to enhance the electrical properties of BCZT ceramics. The co-doped sample with 0.05 mol% Ce and 0.10 mol% Sb shows the optimal properties ($P_{max} = 17.65$ μC cm^{-2}, $P_r = 10.43$ μC cm^{-2}, $E_c = 2.88$ kV cm^{-1}, $d^*_{33} = 417$ pm V^{-1}, $d_{33} = 372$ pC N^{-1}, $T_c = 109.4$ °C). Two reasons were considered for the improvement of ferroelectric and piezoelectric performances. One is the grain coarsening that increases the domain width and size. The other is the restriction of the oxygen vacancy concentration by the donor doped. Therefore, the pinning of domains is reduced and the domain wall motion is promoted simultaneously. In addition, PNRs would be formed with the co-doping of Ce and Sb. The PNRs reduce the coercive field and then facilitate the polarization of the sample. With the addition of dopants, the diffuseness γ was increased from 1.663 to 1.733, indicating a more relaxer ferroelectric characteristic. The increase in T_c indicates the improved stability of the ceramic samples when used at room temperature. All improvements in BCZT ceramics would show their promising applications in electronic devices.

Conflicts of interest

There are no conflicts to declare.

Acknowledgements

This work was financially supported by the University Nursing Program for Young Scholars with Creative Talents in the Heilongjiang Province under Grant No. UNPYSCT-2017095, the Natural Science Foundation of the Heilongjiang Province under

© 2021 The Author(s). Published by the Royal Society of Chemistry

Open Access Article. Published on 12 January 2021. Downloaded on 12/9/2025 6:57:55 AM.
This article is licensed under a Creative Commons Attribution-NonCommercial 3.0 Unported Licence.

Grants No. YQ2019A004 and LH2019F022, the National Natural Science Foundation of China under Grants No. 11444004 and 61372013, and the National Science Foundation for Post-Doctoral Scientists of the Heilongjiang Province under Grant No. LBH-Z19070.

Notes and references

1 B. S. Aronov, E. K. Aikins and D. A. Brown, Increasing piezoelectric effect in radially polarized soft piezoelectric cylinders by pressure treating and its practical applications, *J. Acoust. Soc. Am.*, 2020, **147**(6), 4145–4152.

2 C. Othmani, H. Zhang and C. Lu, Effects of initial stresses on guided wave propagation in multilayered PZT-4/PZT-5A composites: a polynomial expansion approach, *Appl. Math. Model.*, 2020, **78**, 148–168.

3 M. Y. Li, N. Y. Chan and D. Y. Wang, Improved thermal stability of the piezoelectric properties of (Li,Ag)-*co*-modified (K,Na)NbO_3-based ceramics prepared by spark plasma sintering, *J. Am. Ceram. Soc.*, 2017, **100**(7), 1–7.

4 G. S. Xu, H. S. Luo, H. Q. Xu and Z. W. Yin, Third ferroelectric phase in PMNT single crystals near the morphotropic phase boundary composition, *Phys. Rev. B: Condens. Matter Mater. Phys*, 2001, **64**(2), 20102.

5 L. Qing, Y. C. Zhang, G. Jing, Z. Zhou, H. Wang, K. Wang, X. W. Zhang, L. T. Li and J. F. Li, High-performance lead-free piezoelectrics with local structural heterogeneity, *Energy Environ. Sci.*, 2018, **11**(12), 3531–3539.

6 J. G. Wu, Perovskite lead-free piezoelectric ceramics, *J. Appl. Phys.*, 2020, **127**(19), 190901.

7 S. J. Zhang, R. Xia and T. R. Shrout, Modified $(K_{0.5}Na_{0.5})NbO_3$ based lead-free piezoelectrics with broad temperature usage range, *Appl. Phys. Lett.*, 2007, **91**(13), 132913.

8 V. Fruth, L. Mitoseriu, D. Berger, A. lanculescu, C. Matei, S. Preda and M. Zaharescu, Preparation and characterization of $BiFeO_3$ ceramic, *Prog. Solid State Chem.*, 2007, **35**, 193–202.

9 H. H. Gu, K. Zhu, X. P. Pang, B. Shao, J. H. Qiu and H. L. Ji, Synthesis of (K,Na)(Nb,Ta)O_3 lead-free piezoelectric ceramic powders by high temperature mixing method under hydrothermal conditions, *Ceram. Int.*, 2012, **38**(3), 1807–1813.

10 M. Feizpour, H. B. Bafrooei H, R. Hayati and T. Ebadzadeh, Microwave-assisted synthesis and sintering of potassium sodium niobate lead-free piezoelectric ceramics, *Ceram. Int.*, 2014, **40**(1), 871–877.

11 H. W. Lu, J. Q. Lin and H. W. Zheng, Superior ferroelectric properties and fatigue resistance in Tb modified (BaCa)(ZrTi)O_3 film grown on $SrTiO_3$ prepared by pulsed laser deposition, *Appl. Surf. Sci.*, 2020, **527**, 146892.

12 S. Suzuki, S. Yamaguchi, A. Doi, S. Abe, M. Matsuda, T. Nakamura, A. Ando and H. Sano, Effect of alloying Ni inner electrodes on the leakage current degradation of $BaTiO_3$-based multilayer ceramic capacitors, *Appl. Phys. Lett.*, 2020, **116**(13), 132903.

13 N. H. B. Janil, M. H. B. H. Jumali, Z. Z. B. Zainuddin, I. Izzuddin and S. Pojprapai, Penentuan Parameter Optimum bagi Rawatan Pengutuban Elektrik ke atas Seramik-Piezo ($BaTiO_3$) menggunakan Sistem Buatan Sendiri, *Sains Malays.*, 2019, **48**(2), 425–433.

14 H. Takahashi, Y. Numamoto, J. Tani, k. Matsuta, J. H. Qiu and S. Tsurekawa, Lead-Free Barium Titanate Ceramics with Large Piezoelectric Constant Fabricated by Microwave Sintering, *Jpn. J. Appl. Phys.*, 2006, **45**(1), 30–32.

15 H. S. Mallik, I. Fujii, G. P. Khanal, S. Kim, S. Ueno, T. Suzuki and S. Wada, Fabrication of ⟨111⟩-oriented $BaTiO_3$ ceramics by high magnetic field electrophoretic deposition using hexagonal–tetragonal co-existing $BaTiO_3$ powder, *J. Ceram. Soc. Jpn.*, 2020, **128**(8), 469–474.

16 F. Q. Guo, B. H. Zhang, Z. X. Fan, X. Peng, Q. Yang, Y. X. Dong and R. R. Chen, Grain size effects on piezoelectric properties of $BaTiO_3$ ceramics prepared by spark plasma sintering, *J. Mater. Sci.: Mater. Electron.*, 2016, **27**(6), 5967–5971.

17 M. S. Alkathy and K. C. J. Raju, Structural, dielectric, electromechanical, piezoelectric, elastic and ferroelectric properties of lanthanum and sodium co-substituted barium titanate ceramics, *J. Alloys Compd.*, 2018, **45**(8), 10518–10524.

18 T. M. Kamel and G. D. With, Poling of hard ferroelectric PZT ceramics, *J. Eur. Ceram. Soc.*, 2008, **28**(9), 1827–1838.

19 Y. M. Li, W. Chen, Q. Xu, J. Zhou, Y. Wang and H. Sun, Piezoelectric and dielectric properties of CeO_2-doped $Bi_{0.5}Na_{0.44}K_{0.06}TiO_3$ lead-free ceramics, *Ceram. Int.*, 2007, **33**(1), 95–99.

20 B. C. Keswani, S. I. Patil, A. R. James, Y. D. Kolekar and C. V. Ramana, Correlation between Structural, Ferroelectric, Piezoelectric and Dielectric Properties of $Ba_{0.7}Ca_{0.3}TiO_3$–$x$$BaTi_{0.8}Zr_{0.2}O_3$ (x = 0.45, 0.55) Ceramics, *Ceram. Int.*, 2018, **44**, 20921–20928.

21 M. T. Fu, C. X. Li, B. Yang, D. Q. Liu, L. Bian, Y. N. Hong, C. H. Zhang, C. T. Chen and J. Q. Lin, Structure and piezoelectric properties of MnO_2 doped $Ba_{0.985}Ca_{0.005}Ti_{0.98}Sn_{0.02}O_3$ lead-free ceramics, *J. Mater. Sci.: Mater. Electron.*, 2019, **30**, 18950–18958.

22 Y. Liu, Z. Xu, L. J. Liu and F. Li, Morphotropic phase boundary-like properties in a ferroelectric–paraelectric nanocomposite, *J. Appl. Phys.*, 2019, **126**(12), 124102:1–124102:8.

23 M. Budimir, D. Damjanovic and N. Setter, Piezoelectric Response and Free Energy Instability in the Perovskite Crystals $BaTiO_3$, $PbTiO_3$ and Pb(Zr,Ti)O_3, *Phys. Rev. B: Condens. Matter Mater. Phys*, 2006, **73**, 174106.

24 W. F. Liu and X. B. Ren, Large Piezoelectric Effect in Pb-Free Ceramics, *Phys. Rev. Lett.*, 2009, **103**(25), 257602.

25 H. Wu, Y. A. Huang, F. Xu, Y. Q. Duan and Z. P. Yin, Energy Harvesters for Wearable and Stretchable Electronics: From Flexibility to Stretchability, *Adv. Mater.*, 2016, **28**(45), 9881–9919.

26 K. K. Poon, M. C. Wurm, D. M. Evans, M. A. Einarsrud, R. Lutz and J. Glaum, Biocompatibility of (Ba,Ca)(Zr,Ti)O_3 piezoelectric ceramics for bone replacement materials, *J. Biomed. Mater. Res., Part B*, 2019, **108**(4), 1–9.

© 2021 The Author(s). Published by the Royal Society of Chemistry

Open Access Article. Published on 12 January 2021. Downloaded on 12/9/2025 6:57:55 AM.
This article is licensed under a Creative Commons Attribution-NonCommercial 3.0 Unported Licence.

27 L. J. Wang, W. F. Bai, X. Y. Zhao, Y. Q. Ding, S. T. Wu, P. Zheng, P. Li and J. W. Zhai, Influences of rare earth site engineering on piezoelectric and electromechanical response of $(Ba_{0.85}Ca_{0.15})(Zr_{0.1}Ti_{0.9})O_3$ lead-free ceramics, *J. Mater. Sci.: Mater. Electron.*, 2020, **31**(9), 6560–6573.

28 V. Bijalwan, P. Tofel and V. Holcman, Grain size dependence of the microstructures and functional properties of $(Ba_{0.85}Ca_{0.15-x}Ce_x)(Zr_{0.1}Ti_{0.9})O_3$ lead-free piezoelectric ceramics, *J. Asian Ceram. Soc.*, 2018, **6**(4), 384–393.

29 R. Hayati, M. A. Bahrevar, Y. Ganjkhanlou, V. Rojas and J. Koruza, Electromechanical properties of Ce-doped $(Ba_{0.85}Ca_{0.15})(Zr_{0.1}Ti_{0.9})O_3$ lead-free piezoceramics, *J. Adv. Ceram.*, 2019, **8**, 186–195.

30 Q. Xu, D. P. Huang, M. Chen, W. Chen, H. X. Liu and B. H. Kim, Effect of bismuth excess on ferroelectric and piezoelectric properties of a $(Na_{0.5}Bi_{0.5})TiO_3$–$BaTiO_3$ composition near the morphotropic phase boundary, *J. Alloys Compd.*, 2009, **471**(1–2), 310–316.

31 Y. F. Chang, Z. P. Yang, L. R. Xiong, Z. H. Liu and Z. L. Wang, Phase Structure, Microstructure, and Electrical Properties of Sb-Modified (K,Na,Li)(Nb,Ta)O_3 Piezoelectric Ceramics, *J. Am. Ceram. Soc.*, 2010, **91**(7), 2211–2216.

32 D. Lin, K. W. Kwok, K. H. Lam and H. L. W. Chan, Structure, piezoelectric and ferroelectric properties of Li- and Sb-modified $K_{0.5}Na_{0.5}NbO_3$ lead-free ceramics, *J. Phys. D: Appl. Phys.*, 2004, **40**(11), 3500–3505.

33 D. Y. Lu, D. D. Han, X. Y. Sun, X. L. Zhuang and Y. F. Zhang, Raman Evidence for Ba-Site Ce^{3+} in $BaTiO_3$, *Jpn. J. Appl. Phys.*, 2013, **52**(1), 111501.

34 M. Wegmann, L. Watson and A. Hendry, XPS Analysis of Submicrometer Barium Titanate Powder, *J. Am. Ceram. Soc.*, 2004, **87**(3), 371–377.

35 J. Nowotny and M. Rekas, Defect chemistry of $BaTiO_3$, *Solid State Ionics*, 1991, **49**, 135–154.

36 Z. L. Miao, L. Chen, F. Zhou and Q. Wang, Modulation of Resistive Switching Characteristics for Individual $BaTiO_3$ Microfiber by Surface Oxygen Vacancies, *J. Phys. D: Appl. Phys.*, 2017, **51**(2), 025107.

37 G. Arlt and H. Peusens, The dielectric constant of coarse grained $BaTiO_3$ ceramics, *Ferroelectrics*, 1983, **48**(1), 213–224.

38 J. O. Gentner, P. Gerthsen, N. A. Schmidt and R. E. Send, Dielectric losses in ferroelectric ceramics produced by domain-wall motion, *J. Appl. Phys.*, 1978, **49**(8), 4485–4489.

39 H. J. Hwang, T. Nagai, T. Ohji, M. Sando, M. Toriyama and K. Niihara, Curie Temperature Anomaly in Lead Zirconate Titanate/Silver Composites, *J. Am. Ceram. Soc.*, 2010, **81**(3), 709–712.

40 M. Wolters and A. J. Burggraaf, Relaxational polarization and diffuse phase transitions of LA-substituted Pb(Zr,Ti)O_3-ceramics, *Mater. Res. Bull.*, 1975, **10**(5), 417–423.

41 L. J. Liu, Z. Yang, M. X. Wu, L. Fang and C. Z. Hu, Dielectric Properties of $(NaBi_{(1-x)}K_x)_{0.5}Ti_{(1-x)}Nb_xO_3$ Ceramics Fabricated by Mechanical Alloying, *J. Alloys Compd.*, 2010, **507**(1), 196–200.

42 J. G. Hao, W. F. Bai, W. Li and J. W. Zhai, Correlation Between the Microstructure and Electrical Properties in High-Performance $(Ba_{0.85}Ca_{0.15})(Zr_{0.1}Ti_{0.9})O_3$ Lead-Free Piezoelectric Ceramics, *J. Am. Ceram. Soc.*, 2012, **95**(6), 1998–2006.

43 P. Zheng, J. L. Zhang, Y. Q. Tan and C. L. Wang, Grain-size effects on dielectric and piezoelectric properties of poled $BaTiO_3$ ceramics, *Acta Mater.*, 2012, **60**(13–14), 5022–5030.

© 2021 The Author(s). Published by the Royal Society of Chemistry